

Potential use of GLM for Nowcasting and Data Assimilation

**Carolina Araujo¹, Luiz A. T. Machado¹, Jean-François Ribaud¹
and Eder P. Vendrasco¹.**

*¹National Institute of Space Research (INPE), Center for Weather Forecast and Climate
Studies (CPTEC), Rodovia Presidente Dutra, km 40, Cachoeira Paulista, SP, 12 630-
000, Brazil*

Submitted January 2019

Journal Applied Meteorology

Correspondance to: luiz.machado@inpe.br

ABSTRACT

Based on the relationship between lightning and storm microphysics this paper aims to elaborate averaged vertical profiles of polarimetric variables for different classes of lightning density according to the GLM grid and then, evaluate the potential use of these profiles for data assimilation in models of high spatial and temporal resolution. It was used polarimetric variables from a X-band radar located in Campinas-SP and data from the Brazilian Network for the detection of atmospheric discharge (GLM proxy). The main differences between each class averaged profiles for the four variables Z_H , Z_{DR} , K_{DP} and ρ_{HV} was in the region between the surface and the melting layer. For the most intense lightning classes, it was observed signatures associated with higher concentration of ice particles in altitudes, the presence of supercooled drops above the freezing level and the occurrence of larger and more oblate raindrops. To analyze the possible use of the reflectivity profiles as a way to indirectly assimilate GLM information into forecast model it was made a case study using the Weather Research and Forecasting model. It was compared the forecast without assimilation; assimilating reflectivity and wind data; and indirectly assimilating lightning through the profiles. Comparing the 6-h reflectivity forecasts from the run assimilating the profiles and the one assimilating the radar data, the first a better performance apart from the first hour and better allocated more intense systems. Considering the results obtained in this work and all the possibilities offered by the recently launched GLM, the mean reflectivity profiles have potential to contribute to nowcasting systems.

Key words: Lightning, dual-polarization radar, hydrometeor classification, GLM, assimilation.

1. INTRODUCTION

The new generation of geostationary satellites recently launched by the National Oceanic and Atmospheric Administration (NOAA) opens new perspective for nowcasting and data assimilation. The Geostationary Lightning Mapper (GLM) sensor, on board of the GOES-16, is an unprecedented tool and an important resource available for nowcasting (Goodman et al., 2013). The GLM provides electrical discharge observations with wide spatial and temporal coverage over the American continent. The GLM will bring advantages to several areas on meteorology such as nowcasting, modeling, long term lightning observations among many other possibilities. It will allow us to obtain continuous and homogeneous measurements of electrical activity where today there is few or even no surface networks providing lightning information.

Lightning occurrence inside storms is a result of an electric field strong enough to break the air dielectric strength that results on the discharge. The most accepted theory to explain the cloud charging process is based on the non-inductive charging mechanisms (Takahashi, 1978; Saunders et al., 1991), which attempts to explain the relationship between phenomena occurring at the micro and macroscopic level. In a microscale, this theory stipulates that charges separation happens due to the collision between graupels and ice crystals inside the cloud followed by the transport of oppositely charged particle to different cloud regions (Saunders, 2008). The distribution of the charged hydrometers occurs, in a macroscale, due to the dynamic movement. Therefore, it is possible to notice how the cloud microphysical structure plays an essential role on the charge exchange process and to the entire cloud electrification.

Although there are still many gaps to be filled in to better understand all mechanisms involving lightnings, it is evident, that cloud microphysics has strong correlation with the electric discharge (Albrecht et al., 2008). One of the great advantages of dual polarization meteorological radar is related to its capability to provide detailed particles information regarding shape, size, orientation and phase inside the cloud. Some studies have evaluated the relationship between lightning frequency and microphysics using radar reflectivity (Goodman et al., 1988; Williams et al., 1989; Yang and King, 2010) and, they were able to observe various correlations between them, for example, reflectivity thresholds that indicates lighting occurrence. Another work on this correlation, developed by Mattos et al. (2016), analyzed the changes on dual-polarimetric variables according to lightning rate densities and it clearly demonstrated that different lightning ratios are associated with different vertical distributions of hydrometeors inside the storm. Mattos et al. (2016) studied how clouds evolve to thunderstorm and described how cloud microphysics characteristics varies from the moment the first reflectivity is detected to the first Cloud-to-Ground (CG) lightning. The study presented the different patterns of all polarimetric variables according to different density rates and, among the four variables, reflectivity was that present

greatest differences between the lightning categories. In addition, they showed a stable and typical profile for different lightning density.

Another possibility to obtain an even more detailed information regarding the particles distribution inside the cloud is using dual-pol variables within Hydrometeor Classification Algorithms (HCAs). HCAs aim to provide a better identification of the dominant type of hydrometeors associated with a cloud system. There are three different possible approaches to hydrometeor classification: (i) supervised, (ii) unsupervised, and (iii) semi-supervised techniques (Ribaud et al., 2018). In the first one the process relies on a previous correlation between the radar variables and the hydrometeors types based on theoretical models or empirical knowledge. The second approach does not require previous signatures and correlations, it is based on gathering the variables into clusters correspondent to each hydrometeor (Grazioli et al, 2015). Aiming to improve computing costs of using clustering, Besic et al. (2016) developed the semi-supervised method keeping the benefits on not demanding previous information however optimizing the algorithm with a priori correlations.

Multiple meteorological applications could benefit from HCAs such as the microphysical parametrizations in high-resolution numerical weather prediction (NWP) model, allowing a better investigation of the physical relationships between lightning and microphysics (Lang et al, 2004), among others. Ribaud et al. (2016), for example, demonstrated the strong correlation between lightning and microphysical classification data and they showed that lightning initiation was strongly detected mainly in regions of graupel (70% of the cases) and ice (22%) and other hydrometeors (e.g. rain, wet snow) it did not have significant impact on lightning initiation. Comparing lightning density with a cloud structure based on hydrometeor classification can be very useful to understand the electrification processes regarding its vertical microphysical structure.

One challenge related to GLM is to find relationship between lightning and microphysical cloud properties and use it to optimize the ability of numerical weather models for nowcasting of high-impact meteorological events. This short-term forecast models require an accurate representation of the initial condition in a resolution of a few kilometers and with frequent updates (Sun et al., 2014). Since meteorological radars benefit from both high temporal and spatial coverage, derived reflectivity and field winds are naturally the most used on model assimilation in which convection is explicitly solved (Sun, 2005; Hu et al.,2006; Vendrasco, 2015). In the meantime, there are still significant gaps of radar coverage over Brazil and most South American countries and radars are not intercalibrated, thus the GLM presents itself as a significant tool to indirectly provide a homogenous field and well detailed information regarding microphysics inside convective storms over a vast area.

This work is part of the SOS-CHUVA project, which the main goal was to develop research on short-term forecasting, severity detection and precipitation estimation with radar and satellite in high spatial and temporal resolution. SOS CHUVA is a continuity of the CHUVA project (Machado et al., 2014). Therefore, this study focuses on the

relationship between lightning and cloud microphysics, and on the development of averaged vertical profiles of reflectivity associated to the different lightning density. It is based on dual-polarimetric X band radar (XPOL) data and lightning information from surface network as a proxy of GLM density events. The final purpose from this work is to evaluate the possible use of GLM as a way of inferring vertical profiles representative of convective cells as a potential use in data assimilation.

This paper is organized as follows: section 2 presents the data and methodology employed to select the reflectivity averaged vertical profiles and the percentual hydrometeors vertical distribution. Section 3 shows the composite reflectivity profiles for the different lightning density classes, as well as the results using the hydrometeor classification. Section 4 describes the indirect assimilation of the GLM in a case study using the WRF model. Section 5 presents our main conclusions.

2. Data and Methodology

a. Campinas XPOL and Lightning Data

The area and the main instruments of the SOS-CHUVA campaign used in this work are presented in Figure 1. The project is centered in Campinas/SP at 680 m (s. l.) where it is located the XPOL. The X-band radar worked with an angular resolution of 1° , 200 m of radial resolution and 17 elevations. The four polarimetric variables used during the elaboration of the vertical profiles were the reflectivity (Z_H), differential reflectivity (Z_{DR}), specific differential phase (K_{DP}) and correlation coefficient (ρ_{HV}).

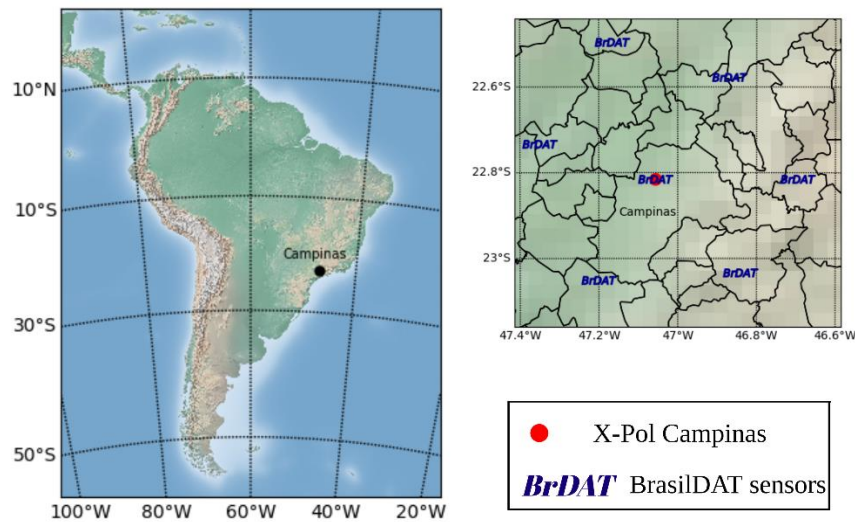


Figure 1. SOS-CHUVA project location on the city of Campinas-SP.

Around the study area are also allocated the Brazilian Network for the Detection of Atmospheric Discharge (BrasilDAT), which use the Earth Networks Total Lightning Network (ENTLN). The sensors operate in the frequency range between 1 Hz and 12 MHz and are designed to detect the electric field measurements resulting from an electric discharge and through time of arrival. Among a set of information regarding the discharge, the sensors provide the occurrence time and geographical locations which are

the data used in this work. BrasilDAT detects both individual pulses, such as intra-cloud (IC), or CGs. As far as the Campinas region is concerned, the lightning network detects in a range of 180 km radius, taking the whole area of the XPOL radar, and its efficiency is about 80% (Nacarato, 2014).

The data used was based on the rain cells measured by the radar in which electrical discharges occurred during the months of November 2016 to March 2017, this period corresponds to the rainy season on Campinas region and are usually associated with a high number of storms. Radiosondes daily conducted in the city of São Paulo, SP, located 90 km from Campinas, showed that during the summer the 0°C isotherm over the region is at approximately 4500 m. As this work proposes to focus on convective events and the assimilation of specific reflectivity profile in cloud resolving models, the profile was computed for the convective clouds only.

b. Combination of lighting and radar observations

The first step to this work consisted in elaborating a lightning density database. It was firstly selected every GLM pixel fully located inside the XPOL range area (Figure 2). The dark gray region represents the non-uniform grid of GLM pixels over the SOS-CHUVA project region. There were 532 pixels considered in this work, they are all fully inside the radar coverage and with an average measurement of 9x9 km².

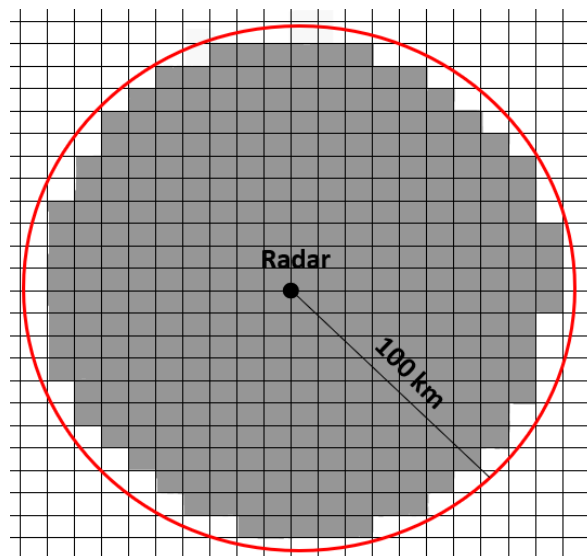


Figure 2. Schematic representation of GLM pixels selected around Campinas region. In gray are the pixels used to calculate the lightning density, which are all fully constrained inside the radar range.

It was selected a 5 minutes time to elaborate the lightning density since during this interval convection does not suffer significant changes, which allows a good representation of the cloud as well as its evolution over time. The density was made counting all lightning that happened in the 5 minutes time interval over the area of each pixel. This period was also selected since it is also compatible with the 10-minute radar scan interval and with the product that will be disseminated by Geonetcast-Americas as well.

Secondly, having defined the integration area and time, each pixel was classified in six different lightning density classes, creating a GLM proxy. For this, it was counted the number of events detected with BrasilDAT that occurred within each pixel over 5 min. The discharge distribution follows a logarithmic pattern, in most of the pixels a small number of lightning was detected and in a minority of them a high density of discharges was observed. To have lightning density classes with statistical relevance, all pixels were assigned in one of the six different classes following a geometric progression, as presented in Table 1.

The stratiform/convective classification proposed by Steiner et al. (1995) was applied on the data aiming to remove lightnings happening in stratiform regions. The classification was made for of each radar gate, according to the reflectivity at 3 km and, analyzed in a grid-Cartesian of CAPPI (Constant Altitude Plan Position Indicator). The last column of Table 1 presents the total amount of lightning events detected for each class during the five months, but only the ones spotted in regions classified as convective.

Table 1. Number of lightning occurrence inside a pixel during 5 minutes for each class.

| Classes | Lightning Density | Number of events |
|----------------|--------------------------|-------------------------|
| Class 1 | 1 | 107,430 |
| Class 2 | 2 to 3 | 202,637 |
| Class 3 | 4 to 7 | 351,417 |
| Class 4 | 8 to 15 | 319,334 |
| Class 5 | 16 to 31 | 382,804 |
| Class 6 | > 32 | 358,485 |

The XPOL variables were combined with the lightning data as follow: for each discharge recorded in a pixel, all the information provided from the radar volume scan constrained in a radius of 1 km around the lightning spot and along 14 km over the vertical were selected. Then, all this information was aggregated according to the class of the pixel in which the lightning occurred. Using BrasilDat data it was possible to locate the closer vertical profile associated with each discharge inside the GLM pixel, keeping the characteristics of the microphysical structure of the storm in the vicinity of the lightning occurrence. The last step was the preparation of the profile itself, the mean value of each XPOL variable were calculated for 1km vertical intervals creating averaged profiles.

c. The Hydrometeor Classification Vertical Distribution

The classification methodology used to do the hydrometeor classification and complement the present study with more detailed observations was based on fuzzy logic. The definition of the polarimetric variables signatures corresponding to each type of hydrometeor was based on the methodology proposed by Dolan and Rutledge (2009) for X-band radar. The first stage of fuzzy logic classification consisted on the elaboration of a T-matrix, in which scattering simulations were run for nine different hydrometeors: rain-weak (DZ), rain (RN), ice crystals (IC), low density (LDG), high density graupel (HDG), vertically aligned ice (VI), melting hail (MH), snow (DS) and wet snow (WS). The last three classes were added according to the parameters proposed by Besic et al. (2016).

The second step was the development of the fuzzy logic for the classification itself. The observations used for this analysis were the four polarimetric variables (Z_H , Z_{DR} , K_{DP} , ρ_{HV}) and the temperature inferred from the radiosondes from São Paulo-.SP It was then calculated the value that represents the correlation degree between the observations and the different type of hydrometeors in a way to retrieve the dominant hydrometeor type within a radar volume. It was used a Gaussian function and a trapezoidal distribution curve for the radar variables and for temperature (Dolan and Rutledge, 2009), respectively. Despite the possibility of coexisting different hydrometeors in a radar gate, the classification assigned to each volume was respective to the hydrometeor that presented the highest correlation score with the set of variables.

Once the classification was already established for each radar gate, the hydrometeors within a 1 km radius around the lightning spot were selected and gathered by class, in a similar spatial distribution as was made to elaborate the average profiles. The HCA percentual distribution was obtained according to the same six electric activity classes, following the principle used in the elaboration of the profiles. However, instead of vertical profiles it was made percentual distribution of different types of hydrometeors along a vertical column associated with different lightning activity.

3. RESULTS

a. The XPOL Profiles

The average profiles for each polarimetric variable and each lightning density class are presented in Figure 4, it is also interesting to notice that it was only used information regarding the storm systems that had good quality XPOL data available.

Overall, the reflectivity profiles (Fig. 3a) significantly increase their difference with height. Knowing that higher Z_H values are proportional to both hydrometeor concentration and the size at power 6, the increase on the reflectivity values observed at altitude along the classes can be explained by the greater amount of particle in altitude as well as the presence of bigger hydrometeors. Greater updrafts, associated with intense convection, allow a bigger rise of moisture and particles to higher levels in the atmosphere, meaning that hydrometeors concentration in altitude can be directly associated with electrical activities density. This relationship is reinforced by the fact that the particles increase at the higher levels are mainly ice particles, which are a crucial element associate for thunderstorm electrification (Takahashi, 1978). Thus, a

higher concentration of ice particles facilitate collision between them, which will intensify the charging mechanisms inside the cloud. Overall, it is expected that classes with more intense electrical density are related with higher ice particles concentration (Mattos et al, 2016).

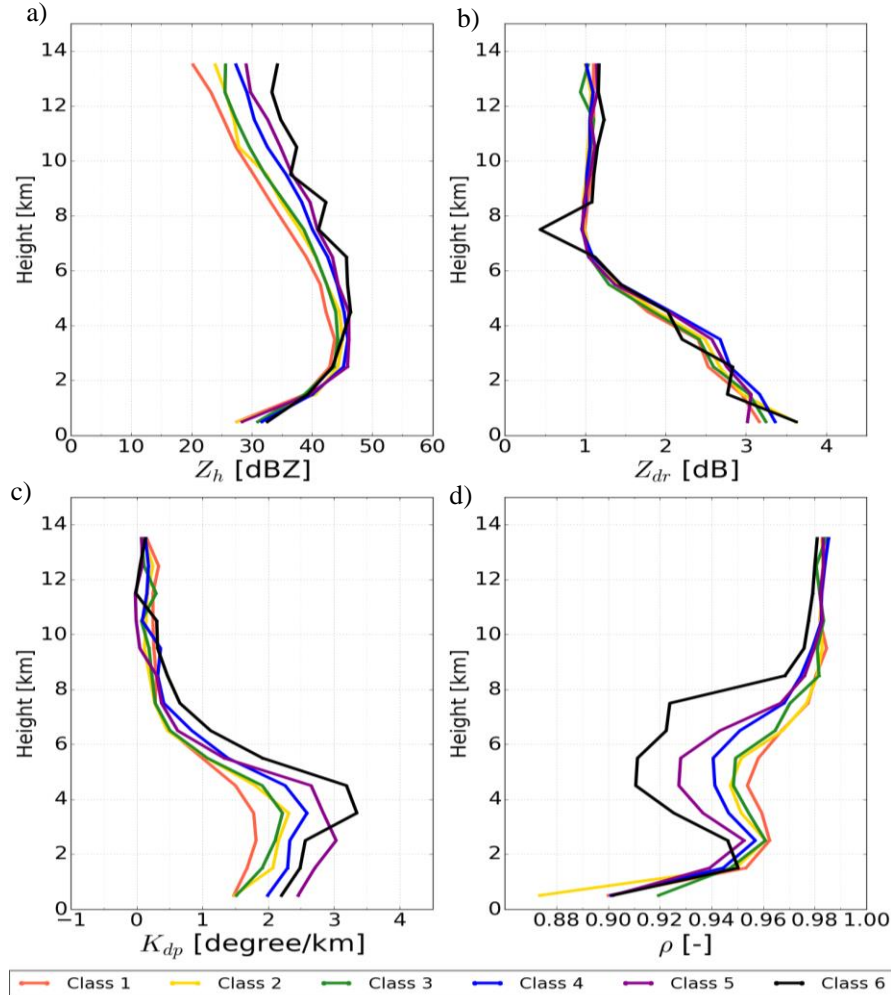


Figure 3. Convective average profiles for each six lightning density classes for: a) Z_H , b) Z_{DR} , c) K_{DP} and d) ρ_{HV} .

The Z_H profiles present their maximum value at 0° C above the melting layer. It is worth noting that the level of maximum reflectivity is higher with increase of the classes. Among other reasons, it may be due to a greater updraft intensity that leads to an increasing concentration of ice particles and supercooled droplets as the lightning density increases. The reflectivity profiles are significantly different above the melting layer. Mattos et al. (2016) found a larger difference among the profiles for different lightning frequency than those observed in this study. The main difference is that their composite was based on the lightning occurrence at the radar profile. In this work the lightning density is based on 9×9 km² area and it does not mean that the number of lightning occurred at the same specific vertical profile reflectivity (VPR), it is possible that several VPRs in the GLM pixel contributed to the specific lightning density. The

results show that at this scale the ice part of all VPRs are quite different along the lightning density classes.

Figure 3b shows the variation of average profiles of Z_{DR} with the classes and, it is possible to notice that Z_{DR} profiles do not show a substantial change between them. However, all Z_{DR} profiles significantly vary their behavior with height, overall Z_{DR} values are higher near the surface than in altitude. In lower levels it is possible to notice a slightly increase of Z_{DR} between the classes proportional to electric activities intensity. This Z_{DR} increase in warm region may indicate the presence of more horizontally aligned particles, such as large oblate droplets. The more intense the updraft the larger ice particles may be, therefore, when melted these particles will contribute to larger droplets formation. Differently from expected, the average profile of Z_{DR} for class 6 did not register the highest values.

Above 4,5 km the six Z_{DR} have profiles a small variability due to the dominant presence of ice particles, which have little variation between the vertical and horizontal diameter. In regions above 6 km all profiles have a similar behavior, all the values are around 1 dB. For all classes at least one electric discharge was observed, i.e. even with different intensities, there was an electric field strong enough to cause lightning which may also lead to more vertical aligned ice particles.

Z_{DR} profiles from Mattos et al. (2016) also had a similar behavior, varying from the base of the cloud and approaching 1dB in colder regions. However, it is interesting to note that, despite the vertical variability present in class 6, the decrease of Z_{DR} above 0° C is not observed. This homogenization of Z_{DR} profiles at altitude may not necessarily be related to the physical aspects of the particles but may be influenced by radar limitations relative to a higher angle required to observe the systems in such higher levels.

Aiming to look at the particles of different water phases it is important to observe K_{DP} values, as shown in the profiles on Figure 3c. Initially, in the warmer regions, below 4.5 km, it is possible to clearly notice an increase in K_{DP} values proportional to electric activity intensity. Above this level, the class 6 profile not only presented the highest values, but also it was the profile that most differed from the others, once it maintained higher values of K_{DP} up to approximately 8 km. This differentiated vertical distribution may be associated with higher particles concentration and with the presence of supercooled droplets in this region, both are related to intense updraft movement associated to class 6. According to Carey and Rutledge (1998), the presence of these supercooled droplets in this region just above the melting layer is a source of graupel embryos, which is deeply related to the cloud electrification process.

All K_{DP} profiles converge to 0° km^{-1} above 8 km. It is interesting to note that the first three profiles have bigger values than the last three between 9 to 10 km. This decrease in K_{DP} is proportional to the lightning density (Ventura et al., 2013) and, together with the increase in Z_H values, they indicate the presence of a large concentration of vertically aligned ice particles. This alignment is explained by the proportional growth electric field intensity, since the more intense the field is the more vertically align the

particles are. This impact of the electric field on the K_{DP} profile can also be clearly observed in Mattos et al. (2016), especially for the case of high discharge density.

A better observation of the 0°C isotherm can be done through the analyze of ρ_{HV} , since it well represents the mixture and phase diversity of hydrometeors present inside storms. In the profiles of Figure 3d, ρ_{HV} almost does not change between the classes over 9 km and all values approach to one. At lower levels the difference between classes is more significant. Smaller values of ρ_{HV} indicate a greater diversity among the hydrometeors found in a certain region. Regardless the class, the lowest ρ_{HV} values observed in all profiles are approximately at 5 km, near the 0°C isotherm where several particles, such as supercooled drops, frozen droplets, graupel and even hailstones can coexist.

The ρ_{HV} profiles variation increase with the classes, i.e, they vary proportional to lightning and convection intensification. Higher levels with lower values of ρ_{HV} may indicate that the melting layer reaches higher levels as the classes increases. This is most evident in the class 6 profile, it has the most distinct behavior not only with respect to the lower values but also because the systems related to this class are apparently strong enough to push a great diversity of hydrometers up. The ρ_{HV} class 6 profile is associated to a such strong upward movement that allows droplets to remain liquid even over the freezing level, which is deeply relates to the lower values of ρ_{HV} observed above 0°C . The ρ_{HV} profiles from Mattos et al. (2016) also showed this relationship between the electric discharge and the higher reach of a more heterogeneous particles distribution.

Lund et al. (2009) also suggested that intense upward currents with a velocity of approximately 5 to 10 ms^{-1} favor the freezing of the hydrometeors in regions close to -10°C , while less intense currents provide better conditions for the hydrometeors to melt. These observations indicate that the predominance of supercooled liquid water in situations of intense electrification is probably a consequence of carried out transport by strong upward currents, which may have promoted a greater mixing and formation of more diverse hydrometeors. This process tends to favor larger graupel formation through riming process, thus it can be a contributor to electric cloud charging through the non-inductive mechanism.

b. The HC Vertical Distribution

Although the polarimetric variables provide a coherent and well detailed result regarding the cloud microphysics, it is not enough detailed to show the hydrometeor nuances inside the system. The HCA provided a more thorough combination of all polarimetric variables which allows a deeper analysis of the correlation between the particles inside the convective clouds and their relationship with electric activity.

The analysis of the Hydrometeor Classification (HC) was made exclusively for the December 3rd case over Campinas. This event was selected owing to the strong precipitation and intense winds that happened on the region. The most intense phase of the thunderstorms occurred between 19 and 20 UTC, however, rain and lightning detection began throughout the region apart from 15 UTC and lasted, with changes in intensity, until shortly after 23 UTC. This event took place due to the presence of a

ridge at high levels and a humidity input brought to the region by the low-level jets. This weather configuration is very common in South America. The system generated intense wind gust of up to 71 km.h^{-1} and hail in some locations.

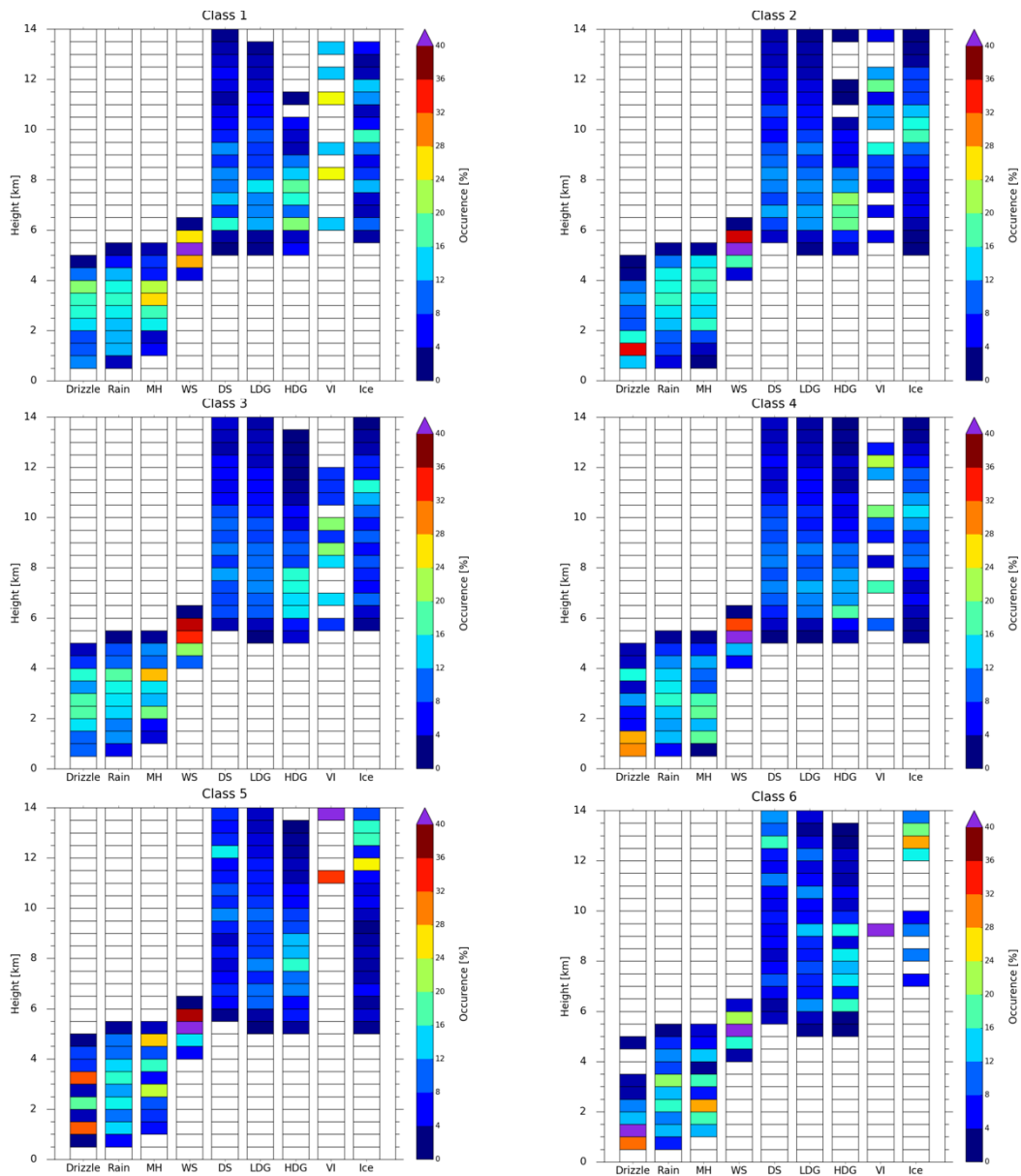


Figure 4. Hydrometeors percental distribution along the vertical for all density classes. Obtained for the case of December 3rd, 2016.

The HC percental distribution are presented in Figure 4. For all six classes is clearly observed the distinct separation of the liquid and solid hydrometeors around 5 km, and it is probably due to the determining role of temperature that plays on the fuzzy logic classification. Note that the classification for the December 3rd event presents a greater number of hydrometeor classes, and it is possible to notice their differences between the electrification classes. One of the most notable variation according to the cloud electrification intensity is the increasing height where the larger concentration of graupel and ice particles are found. In class 1, for example, the maximum graupel concentration is at 7.5 km and the larger amount of ice is found at around 9.5 km, and

for class 6 these maximum concentrations are around 8 km and 13 km respectively. Considering that ice crystal and graupel are the main particles in the cloud electrification process, since they form two regions oppositely charged (ice-negative, graupel-positive). This distance between these regions impacts the electric field strength, once the distance increases it intensifies the electric field strength whereas in within a limit threshold. Regarding the ice particles, it is interesting to notice that in lower density classes they are better distributed along the column, with a not so intense peak occurring between 9 and 10 km. The opposite is observed for higher density classes, where the crystals have their densely concentration peak between 12 and 14 km and, especially in class 6, it is possible to notice that ice is practically totally concentrated in higher regions inside the cloud. The graupel maximum concentration region can show the impact of different convection intensities. In the smaller classes its higher values are between 6 and 7 km and for larger classes it is between 8 and 9 km.

Knowing the behavior of particles within convective systems allows not only a better understanding of the whole system, but also the development of tools and techniques that can contribute to forecast quality, especially when there is a need for a good representation of the systems in a smaller scale. The GLM-proxy lightning density classes seems to be able to identify these typical profiles.

4. A CASE STUDY: Vertical Profiles Assimilation

As described above with the GLM lightning density classes it was possible to establish the average profiles of polarimetric variables or hydrometeor types for each lightning density class. Aiming to evaluate the use of these profiles according to each lightning density class, a test was performed using these lightning density classes for data assimilation with the WRF model. The main goal was to analyze the possible use of these profiles for assimilation purposes and to verify the impact they can have on the quality of short-term forecast. With this regard, the specific event over Campinas region that occurred on December 3, 2016 was considered. Since the assimilation system (WRFDA) control variable for humidity is reflectivity, we used in this evaluation only the average reflectivity profiles.

The reflectivity profiles were assimilated using the WRFDA 3DVar system (Barker et al., 2004), which is the assimilation component of the WRF model (Skamarock, 2008). The WRFDA is a system with strong development on radar data assimilation and it was used this capability to assimilate the averaged reflectivity profiles as it is done for radar data.

The sigma vertical coordinate, that follows the terrain, was used in the model and WRF is currently in operational use in NCEP and CPTEC/INPE. WRF was run at a resolution of 1 km and the physics used was adjusted in a standard pattern defined for all SOS CHUVA case studies: Morrison was used for microphysics parameterization; for longwave and shortwave radiation the RRTMG was selected; the surface layer scheme employed is the revised Monin-Obukhov; the surface parametrization is Noah; and the YSU scheme for the planetary boundary layer.

Three different WRF runs were made for comparison purpose. The first one was done without any assimilation, the second one was done assimilating reflectivity and wind data from the XPOL, according to details found in Vendrasco (2015). In the third round the reflectivity profiles defined by the GLM-proxy classes were assimilated. As already mention, it was only assimilated reflectivity profiles (Z_H) according to the electric discharge density from the GLM proxy field created with BrasilDAT data. The reflectivity assimilation was done indirectly through the conversion of reflectivity into rainwater mixing. It is important to notice that all other configurations of the model were the same for the three runs.

The area selected to insert the profiles was the one used throughout this work (gray region in Fig.2), more specifically the profiles were allocated in the central latitude and longitude of each GLM pixel over the Campinas region. During each hour of the assimilation processes, all the pixels with lightning occurrence were classified according to the discharge density established in Table 1 and then it was assigned to each pixel the average reflectivity profile correspondent to the respectively class. The assimilated profiles were done every hour in four cycles. At each cycle it was assimilated the total pixels where lightning happened during the one hour (60 minutes) preceding the moment the assimilation was made, all profiles inside each pixel with lightning prior one hour before each cycle were assimilated together hourly.

An important point is that by hypothesis it was considered that all discharges occurred in the convective area, which in a way, is a limitation, since some of the discharges may have occurred in the stratiform region. Certainly, with the release of new sensors, such as the Advanced Baseline Imager (ABI), it is possible to considerably improve this procedure using, for example, a convective-stratiform classification and better allocate the average profiles, putting them in regions with minimum brightness temperatures. Therefore, the present tests are as simple as possible, only to evaluate the potential use of this method to reduce the spin up of high temporal resolution models for nowcasting purpose.

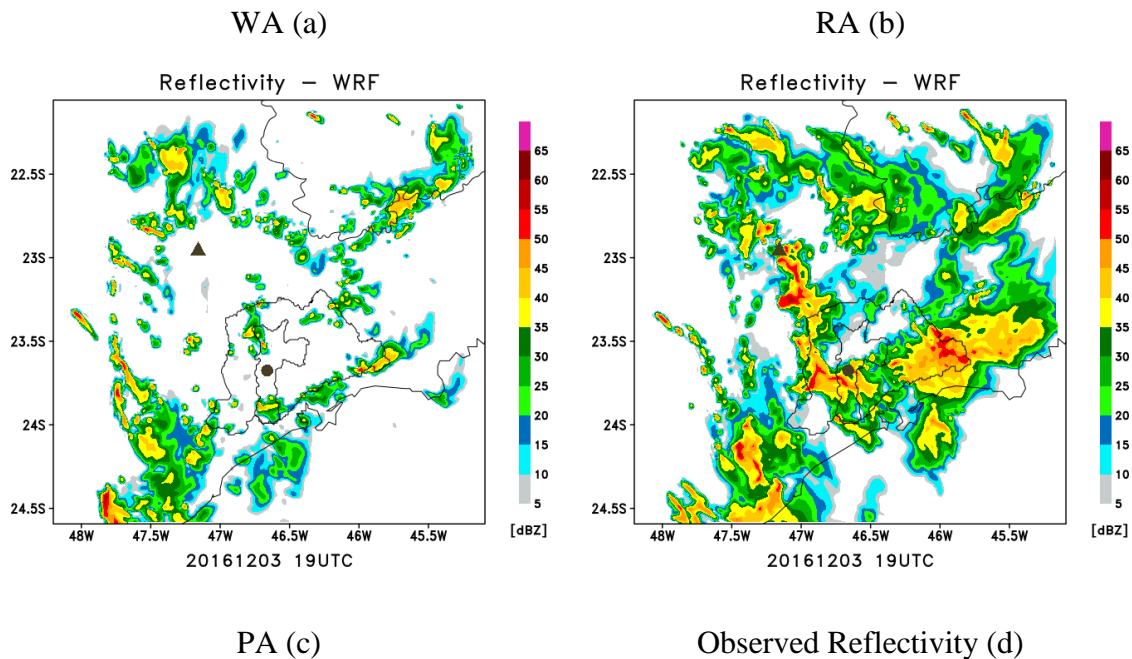
The profiles assimilated was made every hour in four cycles, at 15, 16, 17 and 18 UTC. The control simulation assimilating reflectivity and doppler directly from the radar followed the same procedure. As the rainfall moved out of the XPOL domain the radar data used in this simulation was a S Band, located in São Roque-SP, that largely covered all the region. The discharge intensity increased significantly between 15 and 18 UTC. Between 14 and 15 UTC only 13 GLM pixels were detected within the radar area, consequently only 13 profiles were assimilated at 15 UTC. The model was integrated over an hour and then the second assimilation was made again. The number of GLM pixels increased significantly, and 60 profiles were assimilated at 16 UTC. At 17 UTC 257 profiles were assimilated and in the last cycle, at 18 UTC, 359 profiles were assimilated. From 18 UTC the model ran the forecast for 12h, until 06 UTC 4th December, however the precipitation only lasted until midnight.

The three reflectivity fields from WRF, without assimilation (WA), with radar data assimilation (RA) and the one done with the average reflectivity profiles based on GLM lightning density assimilation (PA) are presented in Figure 5. The S-band radar

provided the data used on the RA forecast. The main goal to run the RA is to compare the PA results with the radar data assimilation in numerical forecasting models, since reflectivity and doppler assimilation are bringing significant improvements to short-term forecast (Sun, 2005, Li et al., 2012; Wang et al. 2016; Vendrasco, 2016).

All model runs allowed to observe that the WA, comparing with the radar, greatly underestimates reflectivity values and poorly places the precipitation over the area. In the same way it is possible to note that both RA and PA have a better performance regarding rain rate and allocation compared to the result WA. In Figure 5, referring to 19 UTC, it is possible to observe a similar behavior between RA and PA fields, and both had problems detecting the precipitation at northwest from Campinas. The field generated with RA (Fig. 5b) showed the more intense reflectivity centers better than PA (Fig. 5c). Observing the progress over time, it is possible to notice that the system moved from the northwest to the southeast between 19 and 22 UTC, and all three runs followed this pattern quite well.

Overall, the WA fields have a significantly lower representation of reflectivity than those generated with assimilation, which is expected, since, assimilating both radar and the GLM proxy are somehow an indicative to the model where convection is happening in the region. Analyzing the radar reflectivity between 19 and 22 UTC it is possible to notice the system motion towards the ocean and to South of Minas Gerais state (Northeast). The fields with assimilation can follow the precipitation until the ocean, but over Minas Gerais both RA and PA do not represent the precipitation so well, especially at 22 UTC, it is probably due to the non-representation of the system to the northwest, which in the radar images appears to be moving toward Minas Gerais.



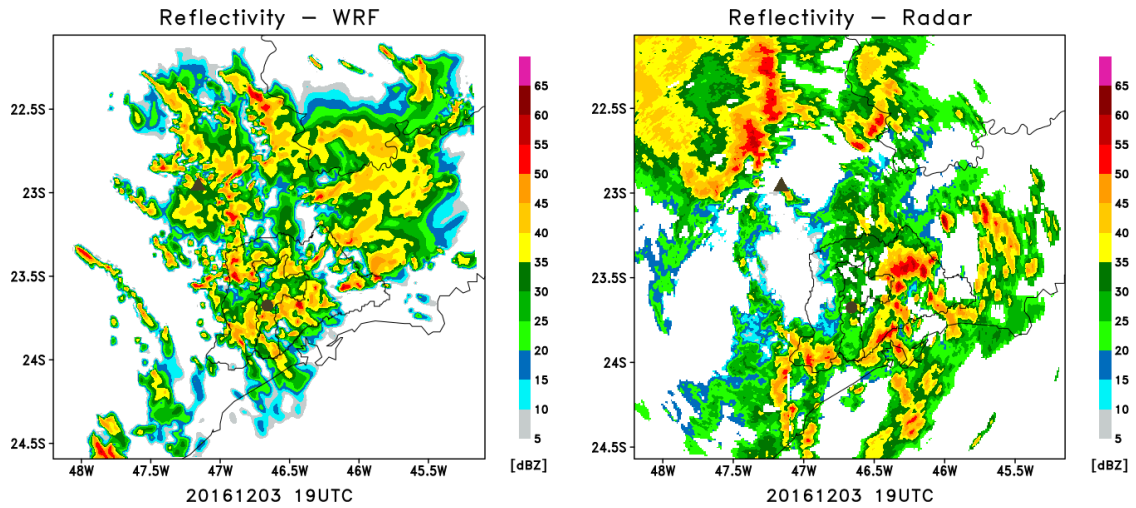
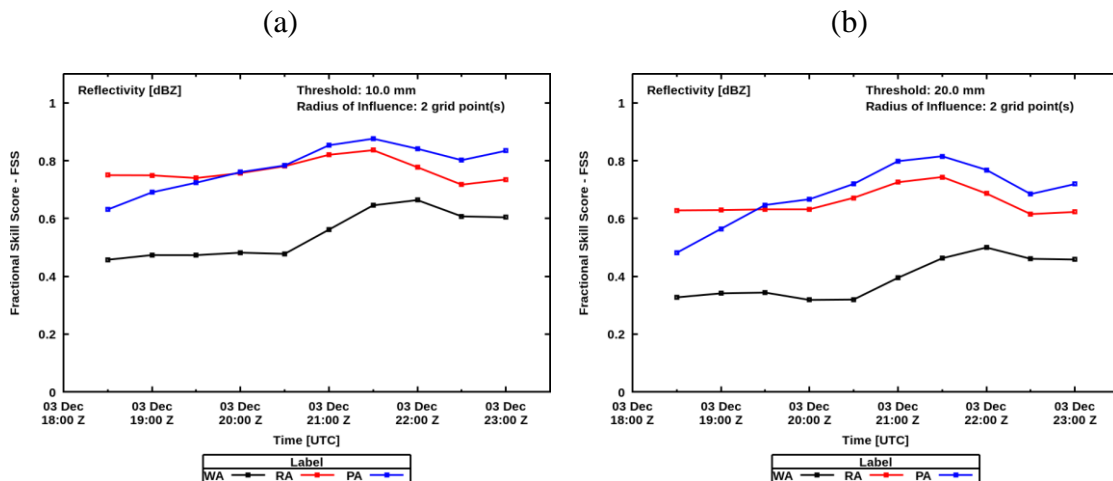


Figure 5. Reflectivity fields at 19 UTC on 03/12/2016 obtained with WRF a) without assimilation, b) radar data assimilation, c) convective profiles assimilation and d) the reflectivity observed by radar.

Despite a slightly similar general behavior between RA and PA fields they present differences that can be better observed through the analysis of Fractional Skill Score (FSS) and Root Mean Square Error (RMSE) indexes over the region and then, to have a better glance on the effect of each assimilation on the model accuracy. The FSS (Fig. 6) evaluates the model regarding the accuracy in predicting a certain limit of reflectivity over an area, which means it does not evaluate the reflectivity value itself. To complement the FSS with a more quantitative analysis, the RMSE (Fig.7) is used as well, since it represents the model accuracy related to the reflectivity magnitude, the smaller the square error the better the result. Comparing the prediction WA with both results obtained with RA and PA, the least ones had a improved performance for the two indexes. The RMSE performance for the PA was worse than for the RA for the first hour of forecast and slightly better than the RA after that. The FSS, for all reflectivity thresholds, had better results with RA during the beginning of the forecast (first hour) and, the assimilation of the profiles provided a more accurate forecast over the following hours.



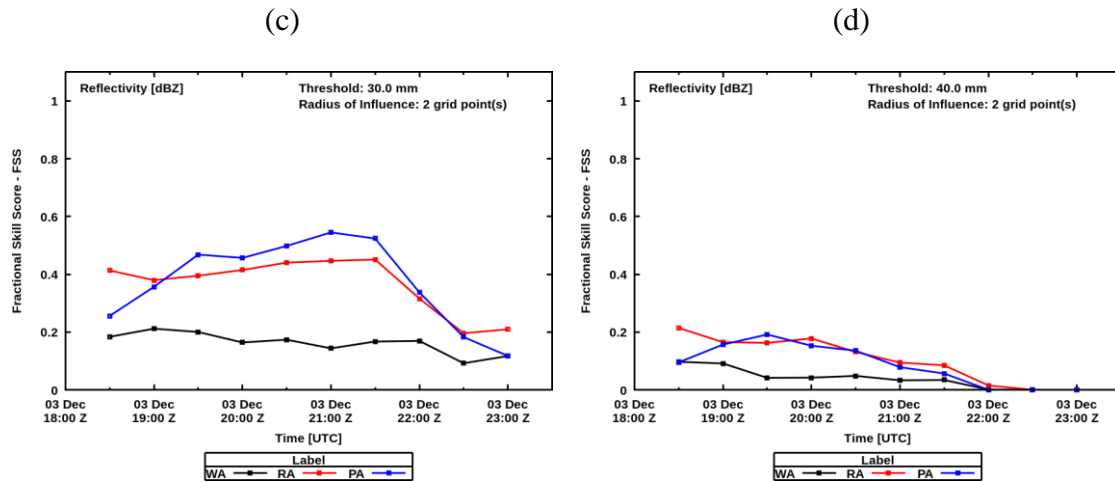


Figure 6. FSS curves for the three products, with no assimilation (black line), radar data assimilation (red line) and convective profiles (blue line), for different minimum reflectivity thresholds a) 10 dBZ, b) 20 dBZ, c) 30 dBZ and d) 40 dBZ.

For a convective reflectivity threshold (40dBZ) all model runs do not perform so well if compared to less intense precipitation, which is expected, since intense precipitation is more difficult for the model to allocate with greater accuracy (Vendrasco, 2015). In this case, both PA and RA had a very similar performance, except during the first hour where RA still maintains a relatively better result.

A joint analysis of these indexes showed that PA did not presented a significant improvement over the first forecast hour in comparison to RA, however PA generally improved the precipitation placement and the intensity prediction from the first simulation hours. A possible explanation for the prevalence of RA in the first hour may be due to the more detailed information provided by the wind data assimilation, which was not considered for PA. Another possible reason is this substantial amount of information that is assimilated in RA if compared to the smoother profiles' information. When using radar data assimilation, the errors can rapidly growth (Vendrasco et al., 2016), thus, the less detailed information from the profiles may have a better communication with the model in a way to generate less noise over time. The results obtained assimilating average profiles were positive although not greatly different from the results with radar data assimilation. PA simulation exceeded the performance of the RA in several moments, especially for cases of intense precipitations (20 and 30 dBZ).

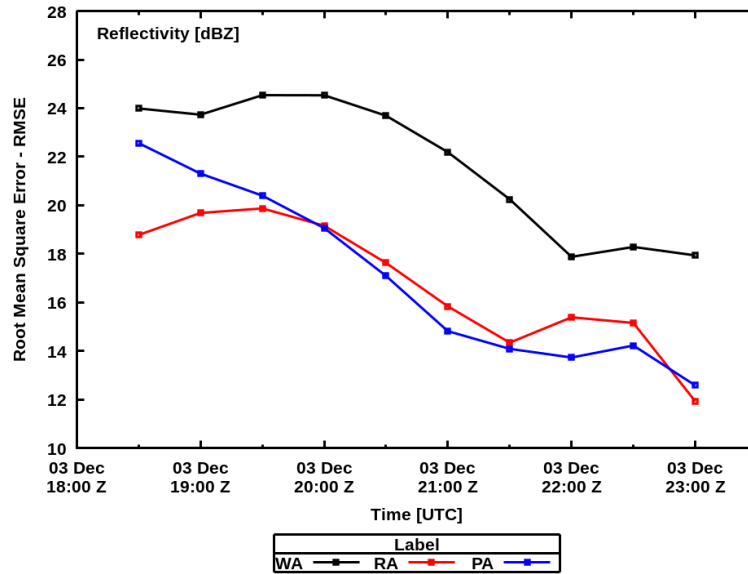


Figure 7. RMSE for the three products, without assimilation (black line), radar assimilation (red line) and convective profiles (blue line).

5. CONCLUSIONS

The main goal of this work was to create an averaged vertical profile of polarimetric variables according to the density of electric activity according to the GLM resolution. The average behavior of the variables around the discharges that occurred in convective regions were analyzed. The variation of the averaged profiles according to the class allowed to observe the correlation of lightning density with microphysical characteristics. Convective systems with higher electrical activity are related with intense updraft within the clouds, which can be observed in certain polarimetric signatures that indicate, for example, the reach of supercooled droplets and graupel at higher levels and, their association with the greater occurrence of electric discharges and ice at the top of the cloud. The profiles also slightly demonstrate signatures of ice alignment in the higher density classes due to the presence of a stronger electric field.

The classifications used to identify cloud types with radar data provided distinct information on lightning occurrence in convective and stratiform regions. It was possible not only to compare the difference between the convective and stratiform profiles, but also to analyze the relevance of obtaining the most representative averaged profile of convective systems.

The different behavior between the six averaged convective profiles may be directly correlated to the cloud characteristics in which the lightning occurred, such as updraft intensity within the cloud and the magnitude of electric field. The most significant differences between the profiles are mainly observed in regions of negative temperatures, which is expected, since it is in this area that the most diverse the hydrometeors phases and ice particles types are. Each updrafts intensity contributes to different configurations of these hydrometeors. In higher levels, although a little subtler, the variation among the classes can be noticed, for example the increase in the average value of reflectivity with lightning density, indicating the presence of a higher

concentration of ice particles in altitude. These intensity variations of electrical activity are the main factor that allows the usage of these profiles as possible indicator of the different convective systems according to their lightning density. The characterization of a typical cloud microphysical profiles as function of the GLM lightning density can be very useful in nowcasting.

In addition, the profiles offer a great opportunity to improve the assimilation process especially in areas without radar coverage. The PA performance tested during this work showed that it may be possible to further improve the profiles assimilation in order to optimize the model accuracy and the spin up reduction. Different mechanisms can be considered and developed seeking this betterment, such as improving the pixel selection and profiles allocation inside the pixels in the model. One important point to highlight is the radar heterogeneity with different calibrations. Assimilating using an average profile make it possible to have larger areas with a homogenous data.

The allocation of convective profiles at the central point of each pixel was adopted as a starting point, however there are other possibilities that can contribute to improve the profile performance in the assimilation process. The center point may not correspond to the location of the convective center and, its extent (the spatial coverage area) may vary from case to case. The use of information provided by ABI channels aboard on the GOES-16 can contribute to better define the closest location to the convective center within the GLM pixel to allocate the convective profile more precisely. For example, an analysis of the cloud top temperature and their coldest regions as well as combining information, such as temperature and effective radius (Rosenfeld et al., 2008) can lead to an optimal allocation spot. The use of ABI can also improve the profiles assimilation results as it can provide a storm stratiform /convective classification within the pixels in order to better select the profile for rain type detected in each pixel. Although not presented in this paper the stratiform profiles were developed as well, their variation is not as distinguish between the six class. Therefore, a possible application of these profiles can be consider, for example, as a standard stratiform profile to be assimilated inside pixels classified as stratiform and the convective profiles assimilated in the pixels classified as convective according to the respective lightning class.

The assimilation of reflectivity profiles, despite being a good indicator, does not bring a very detailed distribution of liquid water inside the cloud. Studies such as Chang et al. (2016), and Li and Mecikalski (2016) demonstrated the positive impact on the short-time prediction caused using more specific information, such as the different microphysical species, on the water distribution inside the cloud. Thus, the use of the hydrometeors classification profiles according to the lightning intensity instead of the radar variables profiles, can be another possible perspective to improve the assimilation process in order to have a better short term forecast. Although not fully explored in this work, it was interesting to notice that HC profiles can distingue characteristics between the classes, such as the higher percentage of the ice crystals and graupel found in higher layers inside systems associated with larger density classes. Another noticed signature is the distance between the region of higher concentration of these two particles, it is also significantly bigger in more intense systems, which is consistent with the presence of a

stronger electric field and the occurrence of a larger amount of lightning. This tool may be quite interesting to be deeper analyzed and developed for further uses.

Overall, the convective profiles obtained in this work were able to represent the variation between systems with different densities of electric discharges. The lightning classes used to produce the profiles, as well as the profiles themselves, can be altered and tested to meet different needs of multiple regions. Although, there is a necessity to improve and better validate these profiles usage, the initial results presented here opens possibilities to develop a set of information that can bring improvements in the quality of the nowcasting and short range forecast for a wide coverage area.

References

Albrecht, R. I., 2008: Eletrificação dos sistemas precipitantes na região Amazônica: Processos físicos e dinâmicos do desenvolvimento de tempestades. PhD thesis — Universidade de São Paulo.

Barker, D. M., W. Huang, Y.-R. Guo, A. J. Bourgeois, and Q. N. Xiao, 2004: A three-dimensional variational (3DVAR) data assimilation system for use with MM5: Implementation and initial results. *Mon. Wea. Rev.*, **132**, 897–914, doi:10.1175/1520-0493(2004)132,0897:ATVDAS.2.0.CO;2.

Besic N., J. Grazioli, M. Gabella, U. Germann, A. Berne, 2016: Hydrometeor classification through statistical clustering of polarimetric radar measurements: a semisupervised approach. *Atmos. Meas. Tech.*, **9**, 4425–4445, 10.5194/amt-9-4425-2016.

Bringi, V.N., R.M. Rasmussen, J. Vivekanandan, 1986: Multiparameter radar measurements in Colorado convective storms. Part I: Graupel melting studies. *J. Atmos. Sci.*, **43**, 2545–2563, [https://doi.org/10.1175/1520-0469\(1986\)043<2564:MRMICC>2.0.CO;2](https://doi.org/10.1175/1520-0469(1986)043<2564:MRMICC>2.0.CO;2).

Carey, L.D. and Rutledge, S.A., 1998: Electrical and multiparameter radar observations of a severe hailstorm. *Journal of Geophysical Research: Atmospheres*, **103**,13979–14000, <https://doi.org/10.1029/97JD02626>.

Chang, S. F.; Y. C. Liou, J. Sun., S. L.Tai, 2016: The implementation of the ice-phase microphysical process into a four-dimensional Variational Doppler Radar Analysis System (VDRAS) and its impact on parameter retrieval and quantitative precipitation nowcasting. *J. Atmos. Sci.*, **73**, 1015–1038, <https://doi.org/10.1175/JAS-D-15-0184.1>.

Dolan, B. and S. A. Rutledge, 2009: A theory-based hydrometeor identification algorithm for X-band polarimetric radars. *J. Atmos. Oceanic Technol.*, **26**,2071–2088, <https://doi.org/10.1175/2009JTECHA1208.1>.

Dolan, B., S.A. Rutledge, S. Lim, V. Chandrasekar, M. Thurai, 2013: A robust C-band hydrometeor identification algorithm and application to a long-term polarimetric radar dataset. *J. Appl. Meteor. Climatol.*, **52**, 2162–2186, <https://doi.org/10.1175/JAMC-D-12-0275.1>.

Goodman, S.J., D. E. Buechler, P.D. Wright, W.D. Rust, 1988: Lightning and precipitation history of a microburst-producing storm. *Geophysical Research Letters*, **15**,1185–1188, <https://doi.org/10.1029/GL015i011p01185>.

- Goodman, S. J., and Coauthors, 2013: The goes-r geostationary lightning mapper (GLM). *Atmospheric Research*, **125**, 34–49, <https://doi.org/10.1016/j.atmosres.2013.01.006>.
- Grazioli, J., D. Tuia, A. Berne.,2015: Hydrometeor classification from polarimetric radar measurements: a clustering approach. *Atmospheric Measurement Techniques*, **8**,149–170, [10.5194/amt-8-149-2015](https://doi.org/10.5194/amt-8-149-2015).
- Hall, M.P.M., J. W. F. Goddard, S. M. Cherry, 1984: Identification of hydrometeors and other targets by dual-polarization radar. *Radio Sci.*, **19**, 132–140, <https://doi.org/10.1029/RS019i001p00132>.
- Höller, H., M. Hagen, P.F. Meischner, N. V. Bringi, J. Hubbert, 1994: Life cycle and precipitation formation in a hybrid-type hailstorm revealed by polarimetric and Doppler radar measurements. *J. Atmos. Sci.*, **51**, 2500-2522, [https://doi.org/10.1175/1520-0469\(1994\)051<2500:LCAPFI>2.0.CO;2](https://doi.org/10.1175/1520-0469(1994)051<2500:LCAPFI>2.0.CO;2).
- Hu, M., M. Xue, J. Gao, K. Brewster., 2006: 3DVAR and cloud analysis with WSR-88D level-II data for the prediction of the Fort Worth, Texas, tornadic thunderstorms. Part II: Impact of radial velocity analysis via 3DVAR. *Mon. Wea. Rev.*, **134**, 699-721, <https://doi.org/10.1175/MWR3093.1>.
- Lang, T. J., S. A. Rutledge, K. C. Wiens, 2004: Origins of positive cloud-to-ground lightning flashes in the stratiform region of a mesoscale convective system. *Geophysical Research Letters*,**31**, <https://doi.org/10.1029/2004GL019823>.
- Li, X. and J. R. Mecikalski., 2010: Assimilation of the dual- polarization Doppler radar data for a convective storm with a warm-rain radar forward operator. *Journal Geophysical Research*, **115**, <https://doi.org/10.1029/2009JD013666>.
- Li, X.; J. R. Mecikalski, D. Posselt, 2017: An ice-phase microphysics forward model and preliminary results of polarimetric radar data assimilation. *Mon. Wea. Rev.*, **145**,683-708, <https://doi.org/10.1029/2004GL019823> .
- Lund, N. R., D. R. Macgorman, T. R. Schuur, M. I. Biggerstaff, W. D. Rust, 2009: Relationships between lightning location and polarimetric radar signatures in a small mesoscale convective system. *Mon. Wea. Rev.*, **137**, 4151-4170, <https://doi.org/10.1175/2009MWR2860.1>.
- Machado, L.A.T, 2014: Projeto Temático: Previsão Imediata de Tempestades Intensas e Entendimento dos Processos Físicos no Interior das Nuvens O SOS- CHUVA (Sistema de Observação e Previsão de Tempo Severo). Access at : <http://chuvaproject.cptec.inpe.br/soschuva/pdf/projeto-soschuva.pdf>
- Mattos, E., L. A. T. Machado, E. Williams, R. Albrecht, 2016: Polarimetric radar characteristics of storms with and without lightning activity. *Journal of Geographic Research: Atmospheres*, **121**, 201–214, <https://doi.org/10.1002/2016JD025142>.
- Naccarato, K. P., O. Pinto, C. D. Sloop, S. Heckman, C. Liu, 2014: Evaluation of BrasilDat relative detection efficiency based on LIS observations and a numeric model. *Proc. IEEE Int. Conf. Lightning Protection,2014*, Shanghai, China. IEEE, 1814-1819.
- Ribaud, J.-F., O. Bousquet, S. Coquillat, H. Al-Sakka, D. Lambert, V. Ducrocq, E. Fontaine, 2015: Evaluation and application of hydrometeor classification algorithm outputs inferred from multi-frequency dual-polarimetric radar observations collected during hymex. *Quarterly Journal of the Royal Meteorological Society*, **142**,95-107, <https://doi.org/10.1002/qj.2589>.
- Ribaud, J. F., O.Bousquet, S. Coquillat, 2016: Relationships between total lightning activity, microphysics and kinematics during the 24 September 2012 HyMeX bow-echo system.

Quarterly Journal of the Royal Meteorological Society, **142**, 298-309, <https://doi.org/10.1002/qj.2756>.

Rubaud, J. F., Machado, L. A. T., Biscaro, T., 2018: X-band dual-polarization radar-based hydrometeor classification for Brazilian tropical precipitation systems. *Atmospheric Measurement Techniques*, <https://doi.org/10.5194/amt-2018-174>, in review, 2018.

Reynolds, S., Brook, M., Gourley, M. F., 1957: Thunderstorm charge separation. *Journal of Meteorology*, **14**, 426–436, [https://doi.org/10.1175/1520-0469\(1957\)014<0426:TCS>2.0.CO;2](https://doi.org/10.1175/1520-0469(1957)014<0426:TCS>2.0.CO;2).

Rosenfeld, D., Woodley, W.L., Lerner, A., Kelman, G., Lindsey, D.T., 2008: Satellite detection of severe convective storms by their retrieved vertical profiles of cloud particle effective radius and thermodynamic phase. *Journal of Geophysical Research: Atmospheres*, **113**, <https://doi.org/10.1029/2007JD008600>.

Saunders, C. P. R., W. D. Keith, R.P. Mitzeka, 1991: The effect of liquid water on thunderstorm charging. *Journal of Geophysical Research*, **96**, 11,007-11, <https://doi.org/10.1029/91JD00970>.

Saunders, C. P. R., 2008: Charge separation mechanisms in clouds. *Space Science Review*, **137**, 335-353.

Skamarock, W.C.; Klemp, J.B.; Dudhia, J.; Gill, D.O.; Barker, D.M.; Duda, M.G.; Huang, X.; Wang, W.; Powers, J.G. A description of the advanced research WRF version 3. National Center for Atmospheric Research, 2008. 125 p. NCAR Technical Note.

Steiner, M., R. A. Houze Jr, S. E. Yuter, 1995: Climatological characterization of three-dimensional storm structure from operational radar and rain gauge data. *J. Appl. Meteor.*, **34**, 1978-2007, [https://doi.org/10.1175/1520-0450\(1995\)034<1978:CCOTDS>2.0.CO;2](https://doi.org/10.1175/1520-0450(1995)034<1978:CCOTDS>2.0.CO;2).

Sun, J., 2006: Convective-scale assimilation of radar data: progress and challenges. *Quarterly Journal of the Royal Meteorological Society*. 131,3439–63, <https://doi.org/10.1256/qj.05.149>.

Sun, J., M. and Coauthors, 2014: Use of NWP for nowcasting convective precipitation: Recent progress and challenges. *Bull. Amer. Meteor. Soc.*, **95**,409-426, <https://doi.org/10.1175/BAMS-D-11-00263.1>.

Takahashi, T.1978: Riming electrification as a charge generation mechanism in Thunderstorms. *Journal of the Atmospheric Sciences*, **35**,1536-1548, [https://doi.org/10.1175/1520-0469\(1978\)035<1536:REAACG>2.0.CO;2](https://doi.org/10.1175/1520-0469(1978)035<1536:REAACG>2.0.CO;2).

Vendrasco, E. P., 2015: The impact of radar data assimilation in the shortrange forecast. PhD Thesis – Instituto Nacional de Pesquisas Espaciais, São José dos Campos, SP, Brasil, 208 pp. Available at: <http://urlib.net/8JMKD3MGP8W/3JDJQU2>

Vendrasco, E. P., J. Sun, D. L. Herdies, and C. F. de Angelis, 2016: Constraining a 3DVAR Radar Data Assimilation System with Large-Scale Analysis to Improve Short-Range Precipitation Forecasts. *J. Appl. Meteor. Climatol.*, **55**, 673–690, <https://doi.org/10.1175/JAMC-D-15-0010.1>.

Ventura, J. F. I., F. Honoré, P. Tabary, P., 2013: X-band polarimetric weather radar observations of a hailstorm. *J. Atmos. Oceanic Technol.*, **30**, 2143–2151, <https://doi.org/10.1175/JTECH-D-12-00243.1>.

Vivekanandan, J., D. S. Zrnic, S. M. Ellis, R. Oye, A. V. Ryzhkov, J. Straka, J., 1999: Cloud microphysics retrieval using S-band dual-polarization radar measurements. *Bull. Amer. Meteor. Soc.*, **80**, 381-388, [https://doi.org/10.1175/1520-0477\(1999\)080<0381:CMRUSB>2.0.CO;2](https://doi.org/10.1175/1520-0477(1999)080<0381:CMRUSB>2.0.CO;2).

Williams, E. R., 1989: The tripole structure of thunderstorms. *Journal of Geophysical Research*, **94**, 13151-13167, <https://doi.org/10.1029/JD094iD11p13151>.

Wang, F., Y. Zhang, H. Liu, W. Yao, Q. Meng, 2016: Characteristics of cloud-to-ground lightning strikes in the stratiform regions of mesoscale convective systems. *Atmospheric Research*, **178**, 207-216, <https://doi.org/10.1016/j.atmosres.2016.03.021>.

Yang, Y. H., P. King, 2010: Investigating the potential of using radar echo reflectivity to nowcast cloud-to-ground lightning initiation over southern Ontario. *Weather and Forecasting*, **25**, 1235-1248, <https://doi.org/10.1175/2010WAF2222387.1>.